Physica Medica 32 (2016) 242–247

Contents lists available at ScienceDirect

Physica Medica

journal homepage: http://www.physicamedica.com

Technical Notes

Characterizing 3D printing in the fabrication of variable density phantoms for quality assurance of radiotherapy

Joseph Madamesila, Philip McGeachy, J. Eduardo Villarreal Barajas, Rao Khan *

Department of Physics Astronomy and Oncology, University of Calgary, Calgary, Alberta T2N 4N2, Canada

ARTICLE INFO

Article history:
Received 18 June 2015
Received in revised form 15 September 2015
Accepted 19 September 2015
Available online 21 October 2015

Keywords:
3D printing
Desktop phantom fabrication
Experimental verification
Dose calculation algorithm

ABSTRACT

Purpose: To present characterization, process flow, and applications of 3D fabricated low density phantoms for radiotherapy quality assurance (QA).
Material and methods: A Rostock 3D printer using polystyrene was employed to print slabs of varying relative electron densities (0.18–0.75). A CT scan was used to calibrate infill-to-density and characterize uniformity of the print. Two printed low relative density rods (0.18, 0.52) were benchmarked against a commercial CT-electron-density phantom. Density scaling of Anisotropic Analytical Algorithm (AAA) was tested with EBT3 film for a 0.57 slab. Gamma criterion of 3% and 3 mm was used for analysis.
Results: 3D printed slabs demonstrated uniformity for densities 0.4–0.75. The printed 0.52 rod had close agreement with the commercial phantom. Dosimetric comparison for 0.57 density slab showed >95% agreement between calculation and measurements.
Conclusion: 3D printing allows fabrication of variable density phantoms for QA needs of a small clinic.

Introduction

The topic of three-dimensional (3D) printing has sparked a great interest in the radiation therapy community by the versatility and growing availability of the medium, as well as the potential fabrication of customized geometries useful for quality assurance or patient treatment. In contrast, commercially available phantoms typically tend to be expensive and not flexible in physical properties when desired. Therefore 3D printing can provide a potential tool catering to the specific needs of the medical physics community.

There are two common types of 3D printers available to researchers and manufacturers: Selective Laser Sintering (SLS) printers and Fused Deposition Modeling (FDM) printers. SLS makes use of a powder mixture in a vat that, when struck with a high-powered laser, creates solid structures within the powder. By doing this layer upon layer a 3D object can be formed without supports and with a larger variety of plastics, metals or glass. Although popular with manufacturers for its versatility the startup cost is very high and is impractical for desktop class prototyping. FDM printing technology is the most popular enthusiast class technique and involves the heating of thermoplastics to liquid form. This is then extruded through a nozzle (the extruder) at the end of the printing arms and deposited layer upon layer onto a flat bed, or onto the previous layer where it fuses with the structure and cools. This makes printing complex geometries and cavities possible by using food and drug safe thermoplastics. The 3D printer used in this technical note is of the FDM type called a Rostock Delta printer that only requires the use of three printing arms to provide the 3 degrees of freedom needed. This lowers the amount of building materials and its complexity while maintaining the capabilities of other FDM desktop class 3D printers.

There have been few publications involving 3D printing in the context of medical physics and radiation therapy. One of the studies investigated the potential use for 3D printing technology in creating a customized bolus for electron radiation treatment. Su et al. used polylactide (PLA) thermoplastic and a Makerbot 3D printer (Makerbot Industries, Brooklyn, NY) to modulate the thickness of the electron bolus resulting in dose conformity of the target volume and a reduction in mean dose to normal tissues nearby [1]. Gear et al. fabricated patient specific phantoms using a Polyjet printer to create molds that were then filled with an ultraviolet curable photopolymer, achieving good correspondence with anatomical references [2]. Ionita et al. performed similar investigations also using Polyjet printing technology to model patient-specific neurovascular anatomy [3]. These investigations use a type of 3D printing which is somewhat expensive. In most of the studies an outer mold is printed to shape the phantom [4,5]. Recently, Solomon et al. have demonstrated the design of anatomically informed textured phantoms for studying imaging noise [6,7]. The phantoms were printed using a multi-material 3D printer employing plastic resins.

* Corresponding author. Department of Physics Astronomy and Oncology, University of Calgary, Alberta T2N 4N2, Canada. Tel.: +14035213088; fax: +14035213327.
E-mail address: rfkhan@ucalgary.ca (R. Khan).

http://dx.doi.org/10.1016/j.ejmp.2015.09.013

The use of 3D fabrication can allow for more complex modeling of human structures [8] and inhomogeneities that cannot be emulated by simple homogeneous phantoms. Of particular interest is dosimetric scalability (via methods such as equivalent path length) and validation of inhomogeneities in treatment planning algorithms.

In this work we have focused on characterizing the 3D printing process by evaluating various parameters which could impact the quality of print with special emphasis on creating entire volumes of phantoms of variable density with high impact polystyrene (HIPS). The 3D printed variable density phantom can simulate a range of densities from low-density lung to adipose tissue, for studies requiring their application. This study focused on producing 3D printed phantoms that fall within the variable lung density range. Further, the ability of the 3D printer to reproduce phantoms used in radiotherapy QC was tested by printing and comparing two 3D low-density rods with ones used in a CT electron density phantom. Lastly, the applicability to radiotherapy QC scenarios was further demonstrated by using 3D printed, low density heterogeneous slabs in a phantom for beam measurements to evaluate the heterogeneity modeling of the dose calculation algorithm Anisotropic Analytical Algorithm (AAA) used in the Eclipse (Varian Medical Systems, Palo Alto, CA) treatment planning system.

Materials and methods

3D printer and process

The 3D printer ORION Delta 3D manufactured by SeeMeCNC Indiana was used in our investigation. ORION is a Rostock delta style printer consisting of 3 motor controlled arms to obtain full three degrees of freedom within a maximum printable cylindrical geometry of 150 mm in diameter and 235 mm in height. The X/Y resolution of the extruder head is ±0.1 mm with a Z resolution of ± 0.0125 mm. Thermoplastics used for printing are fully supported by the 0.5 mm extruder head both in extrusion and temperature (up to a maximum of 245 °C). A glass plate is used as a platform for the print and is heated up to 120 °C to allow for increased adhesion of the hot filament, with temperature varied for different thermoplastics.

Geometric volumes such as rectangular prisms measuring approximately $4 \times 4 \times 2$ cm^3, $10 \times 10 \times 2$ cm^3, and cylindrical rods of dimensions 8 cm tall and 3 cm in diameter were printed in this work. The process involves the creation of stereolithographic (STL) files of the volumes. The files are then compiled into G-Code used to run commands that modulate position, velocity, temperature and extrusion timing of the printer. This code is exported and run either using an external PC connected to the printer's controller board (Arduino, Italy) via USB running 3D printer management software (Matter Control v.1.2), or from exported G-Code files through SD card. For this study the former method was used and interfaced with Matter Control. The Arduino controller was running the latest printing software Repetier (Hot-World GmbH & Co. KG, Germany) v.0.91.

The main parameter of the printer software that controls the final internal mass density of the object is the *infill*, ranging from 0 to 1 as the ratio of printed thermoplastic volume to air volume. Once selected, the infill value is constant throughout the fabricated object and cannot be altered mid-print. Various infill patterns can be used in fabrication including honeycomb, concentric, linear, and grid as described in Impact of various infill patterns on quality. For almost all of the 3D printed phantoms (except for Impact of various infill patterns on quality), we restricted the infill pattern to the most commonly available grid pattern. In all cases, the geometric fidelity of the printed block and rods was verified with CT measurements.

Selection of filament material

Although the printer supports any thermoplastic within the extruder temperature range as a filament material, high impact polystyrene was chosen. The mass density of HIPS (1.07) allows for a density range close to biological tissue even before extrusion. The filament used was 1.75 mm in diameter, white HIPS readily available from many manufacturers with little variation, with each spool costing approximately $40 USD for 250 m.

Polystyrene's chemical composition is $(C_8H_8)_n$ making it ideal for printing tissue-mimicking phantoms versus other thermoplastics that may contain higher Z elements. Although printing with higher or lower density filaments may allow for a wider range of printable densities, the added presence of elements such as silicon can increase complications that can be easily avoided when selecting an appropriate filament material. The usable extrusion temperature of polystyrene is between 220 and 230 °C making HIPS approximate the printing parameters of default acrylonitrile butadiene styrene (ABS) settings. The actual temperature of the extruder during printing was maintained between 228 and 229 °C as controlled by the Arduino controller. A mixture of HIPS and acetone is applied to the cold glass plate before heating to increase adhesion. The heating plate was set to a temperature of 80 °C, despite a recommended HIPS temperature of 115 °C due to the significant amount of time required to heat the plate. Further, excess heat can cause the HIPS to curl if the base structures are too thin. At 80 °C, sufficient adhesion between the polystyrene and glass was achievable while preventing the curling commonly found in high temperature 3D printers.

Phantom infill-to-density calibration

The *infill* of a 3D printer is a parameter that controls the spacing between print lines within the internal structure of an object (the ratio of printed thermoplastic volume to air volume). Calibration blocks of $4 \times 4 \times 2$ cm^3 were printed with the infill range 0.05–1.0 in steps of 0.05 to determine the correlation of infill with the mass density (Fig. 1). The blocks were scanned with a computed tomography (CT) scanner at $0.5 \times 0.5 \times 0.4$ mm^3 resolution. From the CT data a 3D voxel matrix of Hounsfield Unit (HU) values was extracted from the central region of interest inside a given block,

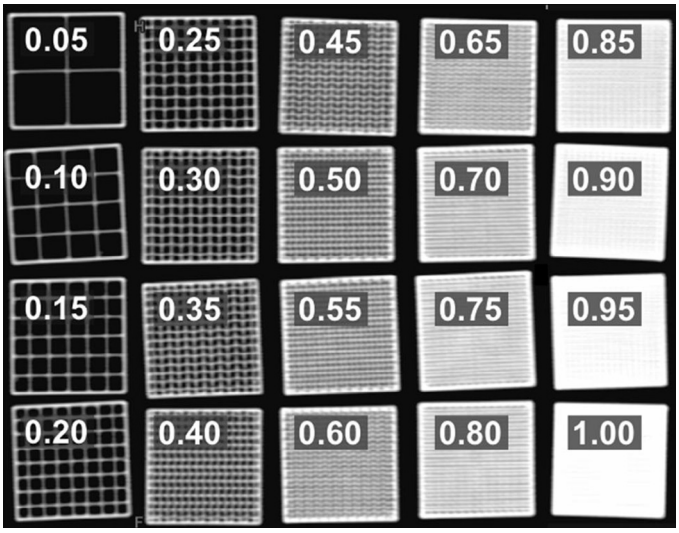

Figure 1. Calibration of the 3D printer infill was performed using a CT scan. The varying infill values used by the 3D printer are superimposed onto their corresponding CT showing the internal structure.

Table 1
Impact of 3D printed infill pattern on relative electron density and HU for infill value of 0.6 with HIPS.

Infill pattern	Relative electron density	Measured Hounsfield Units (HU)
Grid	0.45 ± 0.04	−580 ± 41
Concentric	0.45 ± 0.04	−565 ± 36
Honeycomb	0.31 ± 0.06	−705 ± 63
Lines	0.45 ± 0.01	−565 ± 8
Triangles	0.44 ± 0.07	−576 ± 72

excluding the block exterior. The mass density of the printed blocks was calculated using the HU to electron density calibration. A relationship between the infill parameter and calculated HU (or mass density or relative electron density) could then be obtained by fitting a linear curve to the HU (or mass density or relative electron density) obtained for the different blocks of known infill parameter. This relationship allows one to recreate a phantom of desired density by inputting the corresponding infill value obtained from the fitted linear equation.

Impact of various infill patterns on quality

For a given infill value of 0.6, blocks of $4 \times 4 \times 2$ cm^3 were printed with various infill patterns *grid*, *concentric*, *honeycomb*, *lines*, and *triangles*. The blocks were scanned with the (CT) scanner at $0.5 \times 0.5 \times 0.4$ mm^3 resolution and HUs were extracted as described previously. Using the infill to density calibration, the quality of patterns was evaluated as given in Table 1.

Verification of the calibration

Using an HU-to-electron density phantom CIRS Model 62 (CIRS, Norfolk, VA), two commercially available low-density conical inserts (Lung Low 0.18 ± 0.02 and Lung High 0.52 ± 0.03) were 3D printed. The dimensions of the inserts were first measured and recreated in SolidWorks (Dassault Systèmes, France) version 2015 and exported as an STL file to be read by the printer. The 3D printed inserts were fabricated using the calculated calibration curve (Fig. 3) to closely match the CIRS inserts. CT scans were acquired at $0.34 \times 0.34 \times 0.4$ mm^3 resolution to determine the density and uniformity. CT scans of the 3D printed equivalents can be seen in Fig. 2.

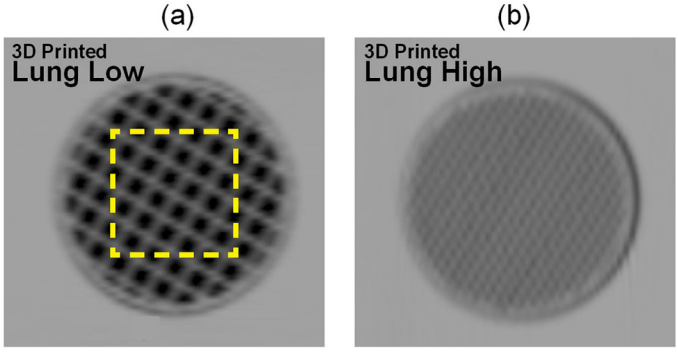

Figure 2. CT scans of 3D printed objects mimicking (a) low density lung (0.18) and (b) high density lung (0.52) using the infill-to-density calibration curve to determine the corresponding infill setting for each object. The yellow dashed box represents the region of interest used to calculate the density of each insert. (For interpretation of the references to color in this figure legend, the reader is referred to the web version of this article.)

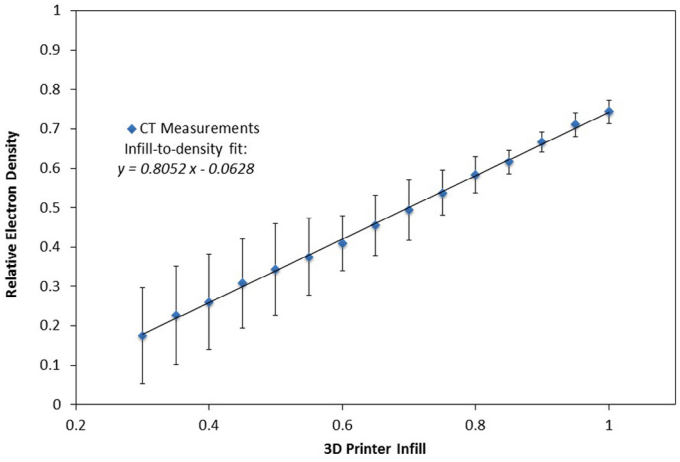

Figure 3. Calibration curve of the 3D printer relating the parameter infill (the ratio of printed thermoplastic volume to air volume) to the measured relative electron density calculated using CT voxel data. The error bars represent one standard deviation of mean; the magnitude of error bars reflects an increased air volume encountered with infill values <0.6.

Dosimetric evaluation of heterogeneous phantom

A test block of $10 \times 10 \times 2.4$ cm^3 was 3D printed with a relative density of 0.57 to evaluate the dose scaling of the Anisotropic Analytical Algorithm (AAA) in the Eclipse treatment planning system. The experimental arrangement is shown in Fig. 5A. The test block was surrounded by a Perspex phantom laterally while Solid Water layers (Gammex-RMI, Middleton, WI) were placed above and below

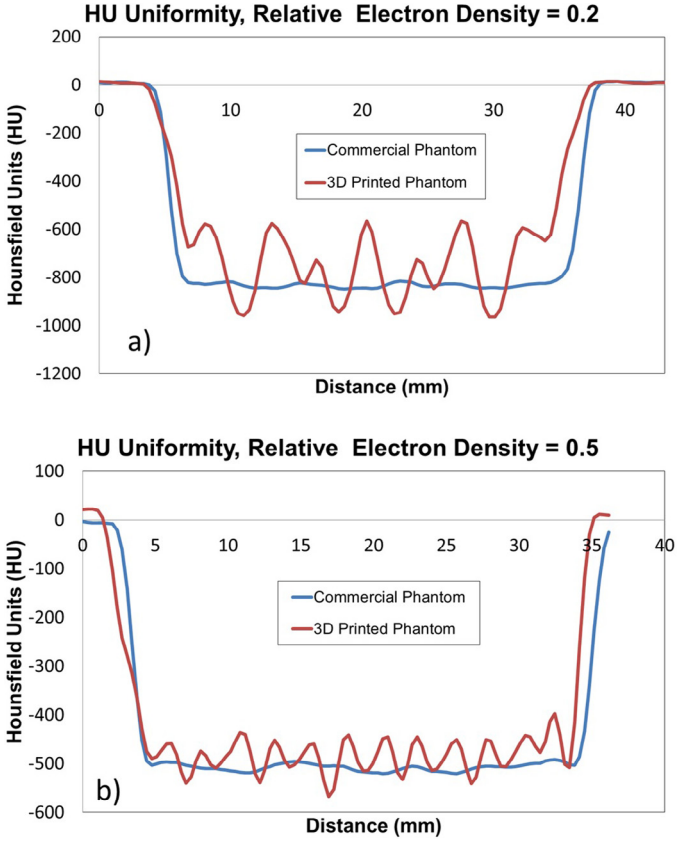

Figure 4. HU line profiles across the 3D printed low relative electron density rod inserts: 0.2 (a) and 0.5 (b).

to provide sufficient buildup and scattering. The test block orientation was labeled for the purpose of reproducibility and alignment between the simulation and the irradiation. A CT was obtained of the phantom and a plan with the corresponding dose was created using the AAA algorithm in Eclipse for a 5×5 cm^2 6 MV clinical photon beam directed along the center of the test block, with an intended 200 cGy delivered at a depth of 4 cm (depth P in Fig. 5). The plan was then delivered on a Varian TrueBeam linear accelerator for the given set, with measurements taken at two depths (P and Q in Fig. 5) using EBT3 film (International Specialty Products Ashland Inc., Covington, KY). The gamma index was calculated with 3%/3 mm criteria to compare the computed AAA dose plane from Eclipse with the measurement obtained from the EBT3 GafChromic film.

Results and discussion

Figure 3 shows the calibration plot obtained by varying the 3D printed infill. The error bars in the data represent one standard deviation of the mean HU value in the region of interest (ROI) as shown in Fig. 2a from the CT voxel data. Larger standard deviations were observed at lower infill values due to the presence of air gaps in the polystyrene mesh. The deviation about the mean increases since large air voxels (0.001293 g/cm^3) are mixed with polystyrene filament voxels of density (1.07 g/cm^3) to create a desired low density volume. This graph also shows that usable infill values are recommended to be above 0.6 (corresponding to a relative electron density of >0.4). Blocks printed with an infill less than 0.6 with HIPS had air gaps ~1.5 mm in the direction parallel to the printer base plate, and may in fact be larger than 1.5 mm in the direction orthogonal to the base plate. This may limit their use for exceedingly low density ranged phantoms. The usefulness may vary from application to application. For dosimetric quality assurance purposes, a very low density object (air gaps > ½ dose grid resolution) may cause ripples in a dosimetric image which may limit the dose computation accuracy, and create phantom alignment and positioning issues relative to the radiation beam.

This calibration curve provides the foundation for all fabricated blocks within this process and can vary depending on the initial density of the thermoplastic and the width of the extruded material during printing. If the objective is to fabricate higher density phantoms through this process, higher density thermoplastics such as ABS should be substituted instead of HIPS.

The impact of varying the infill pattern on the quality of the printed blocks is shown in Table 1. Honeycomb infill failed to reproduce desired density object, instead it resulted in a lower density and large standard deviation. Lines pattern produced an object with the lowest spread, however, it caused issues with the mechanical stability of the printed block.

Measuring the two low-density conical lung inserts, Table 2 summarizes the relative electron density and HU for each insert using the voxel data within the ROI volume as marked by the dashed box (example in Fig. 2). For each print, the exterior shell of the object is created by default 3 layers thick, which can be either cut out of the phantom or excluded from the ROI measurements. The latter approach was preferred in this study in order to avoid causing mechanical instability of the whole object. It also highlights one of the limitations of this particular 3D fabrication process.

Table 2
Electron density phantom and corresponding 3D printed phantom density and HU comparisons.

	Relative electron density	Measured Hounsfield Units (HU)
Lung low insert	0.18 ± 0.02	–826 ± 17
3D printed	0.20 ± 0.11	–794 ± 120
Lung high insert	0.52 ± 0.03	–483 ± 22
3D printed	0.51 ± 0.04	–487 ± 35

HU line profiles are shown in Fig. 4. The 3D printed profile though has ripples on it which are reminiscent of the inherent nature of the printing process used. For the fabricated high-density lung insert (infill of 0.7), there is good agreement with the commercially available insert. This is also in agreement with the calibration curve which shows smaller errors and greater uniformity for infill values >0.6. Although there is agreement in the average density when compared with the commercial insert, the fabricated low-density lung insert (infill of 0.3) has a relatively large amount of air voxels leading to large uncertainties in the HUs. The ripples are produced due to presence of filament-air-filament interfaces produced throughout the 3D printed object. The lower the density of the object, the lower is the frequency of the ripple, which worsens the profile uniformity. The degree of profile uniformity is related to the phantom's directional dependence which renders it sensitive to misalignment relative to the beam center. Thus the type of printer used in the current work can fabricate useful tissue mimicking materials within the density range of approximately 0.4–0.75 g/cm^3 with comparable uniformity to the commercially available lung phantom objects. In Rostock printers, the uniformity for lower density phantoms may be improved if the interior infill can be more finely tuned to stagger layers (i.e. offset each layer by a certain distance or angle to fill air gaps more evenly). The current version of Matter Control provided does not currently allow for such a possibility. This instead results in large air gaps in the direction orthogonal to the printer base plate which is particularly significant for low density phantom fabrication. The ripple effect in printing low density objects can also be reduced by using low density thermoplastics or using the extruders with finer and finer heads, which are not currently available. In the current study, 3D printing was restricted to the grid infill pattern; exploring other patterns might result in a smaller spread.

Dosimetry comparisons are shown in Fig. 5 between the planned and measured doses in the 3D printed heterogeneous slab phantom. Gamma agreement between calculated AAA dose planes and measured EBT3 films is well above 95% for both dose planes (depths P and Q, Fig. 5) for a 6 MV beam. Absolute dose differences near field edges and in penumbra region can rise up to 10%, owing to the limitations of the treatment planning beam model, reproducibility of the experimental setup, EBT3 film uniformity and variable air gaps between various phantom layers.

In all of our irradiations we aligned the phantom using fiducials on the phantoms in order to reproduce the CT based planning setup. If the air-gap between several layers of a phantom can be reliably reproduced, phantoms can be irradiated from any direction, not just with one directional single beam as was demonstrated in our case. One of the potential issues with using 3D printed phantoms with infill factor of <0.6 could be the reproducibility of alignment and set up between simulation and measurement relative to the beam isocenter. For small stereotactic irradiation fields with dimensions comparable to the spacing of air pockets (very low density objects) in the phantom dosimetry would be highly sensitive to the field alignment and field set up. For stereotactic fields and very low density 3D fabricated phantoms, the dosimetric quality assurance would become a challenging task.

Through this work we have characterized and explored the 3D fabrication process on a Rostock delta 3D printing device. Using an infill-to-electron density calibration plot, phantom objects from 0.4 to 0.75 can be created (corresponding to an infill of 0.6–1.0). Further, this work demonstrates that the custom fabrication of low-density phantoms can be used in the evaluation of dose calculation algorithms such as AAA. A major limitation of the 3D printer used in this study was the use of one single infill, which remains constant throughout the printing process. This limits the fabrication of a

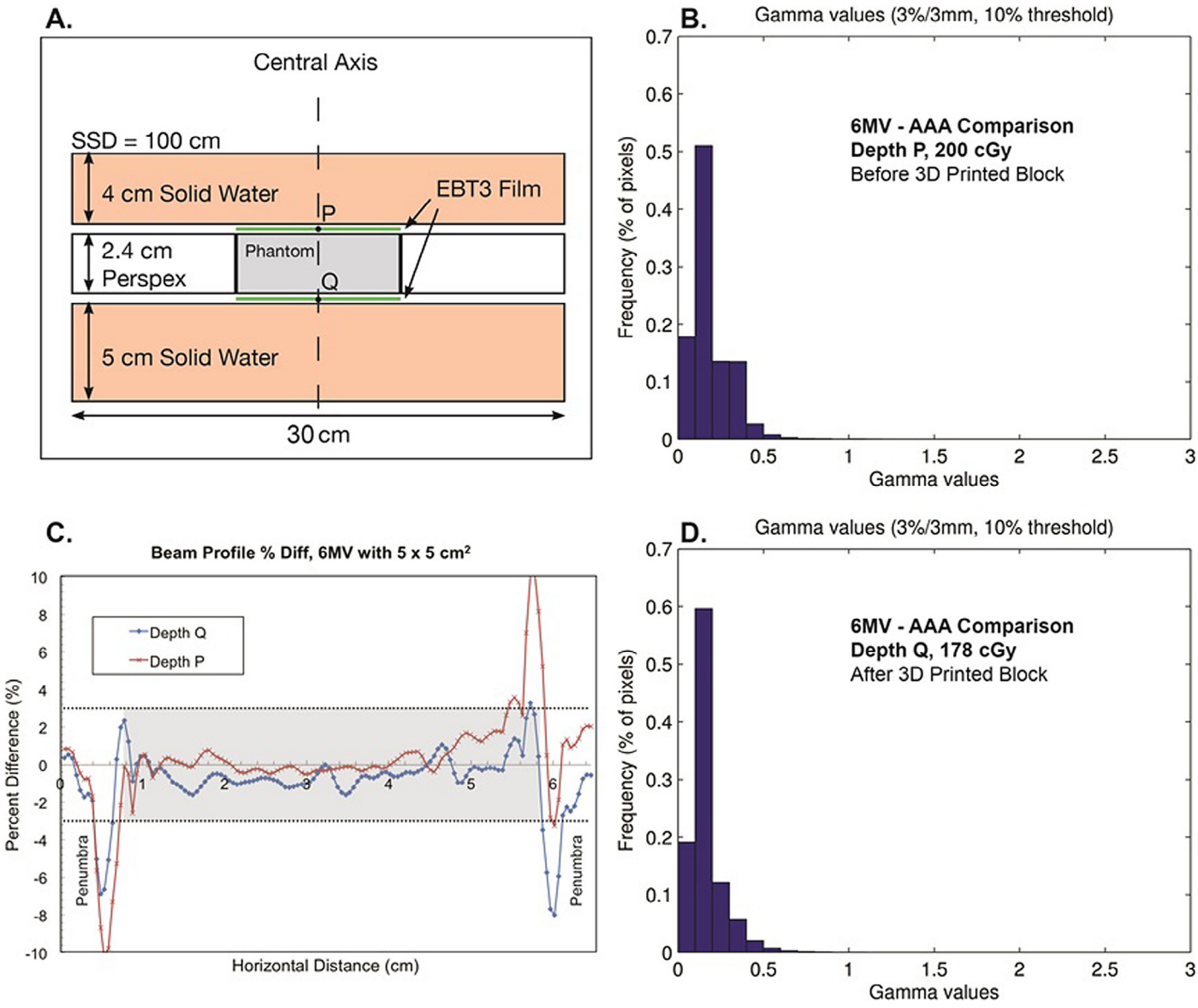

Figure 5. (A) Schematic showing the arrangement of Solid Water and Perspex for buildup and scattering around the printed phantom, along with EBT3 film placement (both above and below). The fabricated block has a measured relative electron density of 0.57 ± 0.05. (B) 3%/3 mm gamma histograms for dosimetric verification of 3D printed blocks at depth P. (C) Beam profile percent difference between AAA and EBT3 film measurements. (D) 3%/3 mm gamma histogram for the lower dose plane at depth Q.

particular object to a single density; an object with a variable density would not be possible in single printing process. The major methodological difference from previous studies that employed 3D printing technology is that those studies involved printing watertight shells filled with liquid composites of fixed density [4]. Our presented method instead involves printing a solid interior that can be varied to modulate density, and describes the challenges arising from therein.

We verified the geometric fidelity for all of the 3D printed blocks and rods, the dimensions obtained from the CT scans were reproducible within the in-plane and slice resolution of the CT scans.

3D printing can be used for variable density phantoms that are inexpensive, scalable to complex geometry, and customized to suit the needs of the experimenter. The advantages of 3D printing are: (i) the low capital and consumable cost of the technology, (ii) the flexibility of printing various geometries and relative electron densities and (iii) the reproducibility of the 3D printed objects. Some of the printing costs have been summarized in Table 3.

The cost of the 3D printer used in this study was approximately $1000 USD, with materials readily available at reasonable prices <$100 USD. The software used is freely available, either through the manufacturer or through open sourced programs for both the 3D

Table 3
3D printing time and resource use excluding capital costs. Ready to print corresponds to a heated glass base plate of 80 °C and extruder of 228 °C from room temperature taking approximately 13 min. Approximate retail cost of HIPS for a 250 m coil is $40 USD.

Volume (cm^3)	Print time	Filament length used (m)	Approximate material cost (USD – $)
1.0	9 min 15 s	0.15	0.02
3.0	23 min 28 s	0.32	0.05
8.0	54 min 34 s	0.80	0.13
100.0	3 h 52 min	8.84	1.41

printer controller and CAD software. The learning curve is relatively low and our method can be employed quickly and efficiently. Current studies with the 3D printer involve the scanning and reproduction of breast seromas for breast brachytherapy and the possible modeling of patient specific inhomogeneities for use in intensity modulate radiation therapy (IMRT) quality assurance. The possible applications of 3D printing are actively being explored by the medical physics community and are of practical interest to small clinics that may benefit from the technology.

Conclusions

3D printing provides a viable and inexpensive method of fabricating variable density solid phantoms. The Rostock delta type desktop 3D printer can be used to create polystyrene phantoms with relative electron densities between 0.75. Although the 3D printed objects contain ripples, they were found to have reasonable uniformity comparable to commercially available high-density lung phantoms. This process provides tools to the radiation therapy community always in need of special purpose custom phantom objects at minimal cost and resources.

Acknowledgements

The authors would like to thank Mr. Rodolfo Zavan from University of São Paulo, São Carlos, SP, Brazil for providing technical expertise in phantom printing and useful discussions in this work. We would also like to acknowledge technical support from Mr. Leo Mariarity and Allan Michaud from the Cancer Centre Machine shop.

References

[1] Su S, Moran K, Robar JL. Design and production of 3D printed bolus for electron radiation therapy. J Appl Clin Med Phys 2014;15:194–211.
[2] Gear JI, Long C, Rushforth D, Chittenden SJ, Cummings C, Flux GD. Development of patient-specific molecular imaging phantoms using a 3D printer. Med Phys 2014;41:082502.
[3] Ionita C, Mokin M, Varble N, Bednarek DR, Xiang J, Snyder AH, et al. Challenges and limitations of patient-specific vascular phantom fabrication using 3D Polyjet printing. In Medical Imaging 2014: Biomedical Applications in Molecular, Structural, and Functional Imaging: Proc SPIE Int Soc Opt Eng. March 13; 9038: 90380M, 2014.
[4] Ehler E, Barney B, Higgins P, Dusenbery KE. Patient specific 3D printed phantom for IMRT quality assurance. Phys Med Biol 2014;59:5763–73.
[5] Bieniosek M, Lee B, Levin C. 3D printing for cost-effective, customized, reusable multi-modality imaging phantoms. In Nuclear Science Symposium and Medical Imaging Conference: Beyond Imagination of Future Science, Seoul, Korea. 2013, doi:10.1109/NSSMIC.2013.6829187.
[6] Solomon J, Samei E. Quantum noise properties of CT images with anatomical textured backgrounds across reconstruction algorithms: FBP and SAFIRE. Med Phys 2014;41:091908. doi:10.1118/1.4893497.
[7] Solomon J, Mileto A, Ramirez-Girald JC, Samei E. Diagnostic performance of an advanced modeled iterative reconstruction algorithm for low-contrast detectability with a third-generation dual-source multidetector ct scanner: potential for radiation dose. Radiology 2015;275:735–45.
[8] Burfeindt MJ, Colgan TJ, Owen R, Shea JD, Behdad N, Van Veen BD. MRI-derived 3D-printed breast phantom for microwave breast imaging validation. IEEE Antennas Wirel Propag Lett 2013;10:1–4.